ruhr.paD
UA Ruhr Zentrum für
partielle Differentialgleichungen

A Bloch wave numerical scheme for scattering problems in periodic wave-guides

T. Dohnal and B. Schweizer

Preprint 2017-08

technische universität
dortmund

A Bloch wave numerical scheme for scattering problems in periodic wave-guides

Tomáš Dohnal, Ben Schweizer

Preprint 2017-03 August 2017

Fakultät für Mathematik
Technische Universität Dortmund
Vogelpothsweg 87
44227 Dortmund

tu-dortmund.de/MathPreprints

A Bloch wave numerical scheme for scattering problems in periodic wave-guides

Tomáš Dohnal and Ben Schweizer[1]

August 1, 2017

Abstract: We present a new numerical scheme to solve the Helmholtz equation in a wave-guide. We consider a medium that is bounded in the x_2-direction, unbounded in the x_1-direction and ε-periodic for large $|x_1|$, allowing different media on the left and on the right. We suggest a new numerical method that is based on a truncation of the domain and the use of Bloch wave ansatz functions in radiation boxes. We prove the existence and a stability estimate for the infinite dimensional version of the proposed problem. The scheme is tested on several interfaces of homogeneous and periodic media and it is used to investigate the effect of negative refraction at the interface of a photonic crystal with a positive effective refractive index.

Key-words: Helmholtz equation, radiation condition, locally periodic media, Bloch waves, negative refraction

MSC: 78A40, 35J25

1 Introduction

Acoustic, elastic, and electromagnetic waves are of quite different nature, but in many geometries of practical relevance, they can all be described by the linear wave equation of second order. If we are interested in the distribution of the wave intensity in a domain $\Omega \subset \mathbb{R}^n$ after a transitional time, we have to solve the time harmonic problem, which is the Helmholtz equation

$$-\nabla \cdot (a \nabla u) = \omega^2 u + f \qquad \text{in } \Omega\,. \tag{1.1}$$

In this equation, $f : \Omega \to \mathbb{R}$ is a source, the positive coefficient field $a : \Omega \to \mathbb{R}$ describes the properties of the medium, we assume that a equals an ε-periodic function $a_+(x)$ on the right of a bounded region and an ε-periodic function $a_-(x)$ on the left. The periodicity $\varepsilon > 0$ and the frequency $\omega > 0$ are given, we consider them as fixed parameters throughout this work. The aim is to find the solution $u : \Omega \to \mathbb{C}$ to equation (1.1).

[1]Technische Universität Dortmund, Fakultät für Mathematik, Vogelpothsweg 87, D-44227 Dortmund, Germany. tomas.dohnal@tu-dortmund.de and ben.schweizer@tu-dortmund.de

We are interested in the analysis of wave-guides. Restricting to the two-dimensional case for simplicity, we consider the infinite strip $\Omega := \mathbb{R} \times (0, H)$ with the height $H > 0$. It remains to choose boundary conditions. The main difficulty comes from the radiation conditions that have to be imposed for $x_1 \to \pm\infty$. In contrast, the analysis is essentially independent of the boundary condition on the lateral boundary $(\mathbb{R} \times \{0\}) \cup (\mathbb{R} \times \{H\})$. To make a choice, we work with periodicity conditions as in [24]: values and derivatives coincide at $(x_1, 0) \in \mathbb{R} \times \{0\}$ and $(x_1, H) \in \mathbb{R} \times \{H\}$.

Radiation condition. At the lateral boundaries, for $x_1 \to \pm\infty$, we have to impose a radiation condition. It is not an easy task to formulate the radiation condition in a wave-guide. For a periodic semi-infinite wave-guide, a condition was formulated and analyzed in [15], similarly, the periodic wave-guide was analyzed in [12, 19], a wave-guide with different coefficients in the two infinite directions was analyzed in [24]. The latter publication provides a the uniqueness result for the suggested radiation condition. It is this radiation condition which we base our numerical scheme on. Let us formulate the following fact in order to illustrate the complexity of the wave-guide problem (1.1). Let the coefficients a be real and bounded from below by a positive number a_0. Furthermore, assume that a is ε-periodic on $x_1 < 0$ and on $x_1 > 0$. Let the source $f : \Omega \to \mathbb{R}$ of class $L^2(\Omega)$ have a bounded support. Open question: Does (1.1) possess a radiating solution u?

In the above question we avoided the precise formulation of the radiation condition – this is adequate since the different forms of radiation conditions in a periodic wave-guide are essentially equivalent. The form of the radiation condition that was suggested in [24] can be written as

$$\fint_{RY_\varepsilon} \left| \Pi^+_{<0}(\{u\}^+_{R,R}) \right|^2 \to 0 \quad \text{as} \quad R \to \infty\,. \tag{1.2}$$

The condition uses the periodicity cell $Y_\varepsilon = (0, \varepsilon)^2$, the function $\{u\}^+_{R,L}$, which is the restriction of u (periodically extended in the vertical direction) to the domain $\varepsilon(R, R+L) \times \varepsilon(0, R)$. For large R, we hence consider the solution u on the far right. Note that we use here boxes of width εL at position εR, while only $L = R$ was considered in [24]. The symbol $\Pi^+_{<0}$ denotes the projection of the argument (which is a function on a square in $\mathbb{R}^2$) onto the space spanned by left-going Bloch waves, i.e. Bloch waves for which the first component of the Poynting vector is negative. The superscript "+" indicates that the Bloch waves are calculated for the periodic coefficient a of the right half-cylinder. The symbol $\fint$ denotes the mean value integral, $\fint_A f := |A|^{-1} \int_A f$. A condition analogous to (1.2) with a projection onto right-going waves must be imposed on the left.

The aim of this contribution is to introduce and to analyze a numerical scheme that can be used to solve the wave-guide problem.

1.1 An approach based on (1.2)

The numerical problem must be formulated in a bounded domain. Furthermore, as in many other related approaches, we must additionally introduce a absorption coefficient $\delta \geq 0$. Our analytical results will only cover the case $\delta > 0$, but practical experience shows that the numerical scheme works well also for $\delta = 0$.

The truncation is performed with two positive integer parameters $R, L \in \mathbb{N}$. We use the inner domain $\Omega_R := (-R\varepsilon, R\varepsilon) \times (0,H)_\sharp$ with $H = \varepsilon K$, $K \in \mathbb{N}$, and the extended domain $\Omega_{R+L} := (-(R+L)\varepsilon, (R+L)\varepsilon) \times (0,H)_\sharp$, the symbol $\sharp$ indicates that we demand periodicity conditions in vertical direction. In the following we suppress the dependencies on $\delta > 0$ and $L > 0$, and denote the unknown function on the truncated domain as $u = u_R : \Omega_{R+L} \to \mathbb{C}$. We impose that u satisfies the Helmholtz equation on the inner domain with the absorption parameter δ:

$$-\nabla \cdot (a\nabla u) = \omega^2(1+\mathrm{i}\delta)u + f \qquad \text{in } \Omega_R\,. \tag{1.3}$$

In order to formulate the radiation condition, we use the positive parameter $L > 0$ and consider the radiation boxes $W^+_{R,L} := \varepsilon(R, R+L) \times (0,H)_\sharp$ and $W^-_{R,L} := \varepsilon(-(R+L), -R) \times (0,H)_\sharp$ as sketched in Figure 1. The restrictions of a function $u : \Omega_{R+L} \to$

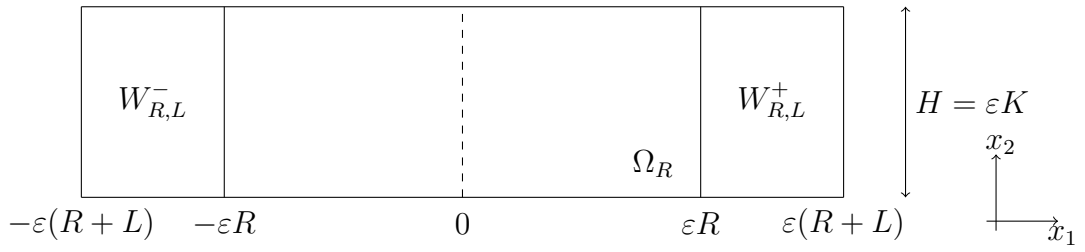

Figure 1: Geometry of the truncated domain

$\mathbb{C}$ to these two rectangles are denoted as $\{u\}^+_{R,L}$ and $\{u\}^-_{R,L}$. More precisely, we additionally shift the lower left corner to the origin and set, for $x_1 \in [0, \varepsilon L)$ and $x_2 \in [0,H)$,

$$\{u\}^+_{R,L}(x_1,x_2) := u(\varepsilon R + x_1, x_2)\,, \quad \{u\}^-_{R,L}(x_1,x_2) := u(-\varepsilon(R+L) + x_1, x_2)\,.$$

We emphasize that the radiation boxes have width εL and are positioned at $\pm\varepsilon R$, while we restricted ourselves to $L = R$ in [24] to simplify notations. The idea is now to impose (1.2) and its counterpart on the left hand side in a strong form at a finite distance; in this first attempt we demand

$$\Pi^+_{<0}(\{u\}^+_{R,L}) = 0 \qquad \text{and} \qquad \Pi^-_{>0}(\{u\}^-_{R,L}) = 0\,. \tag{1.4}$$

The projections are defined below in Definition 2.3. Condition (1.4) expresses that, in the right radiation box $W^+_{R,L}$, the solution does not contain left-going waves, and, in the left radiation box $W^-_{R,L}$, the solution does not contain right-going waves.

Coupling conditions across interfaces. We finally have to demand conditions along the two interior interfaces $\Gamma^+_R := \overline{\Omega_R} \cap \overline{W^+_{R,L}} = \{\varepsilon R\} \times (0,H)_\sharp$ and $\Gamma^-_R := \overline{\Omega_R} \cap \overline{W^-_{R,L}} = \{-\varepsilon R\} \times (0,H)_\sharp$. We impose on u the weak continuity condition

$$u \in H^1(\Omega_{R+L})\,. \tag{1.5}$$

A second condition is needed to replace the continuity of the flux, which may be expressed as

$$[e_1 \cdot a\nabla u]_{\Gamma^\pm_R} = 0\,, \tag{1.6}$$

where the bracket $[.]_{\Gamma_R^\pm}$ denotes the jump of a function across the interface $\Gamma_R^\pm$.

Let us assume that the problem parameters a, ω, δ, and the truncation parameters R and L are fixed. Our first attempt to define a truncated problem is the following.

(P_0): Given f, find u that satisfies (1.3)–(1.6).

Warning: Problem (P_0) is not a useful truncated problem since it does not contain a partial differential equation in the boxes $W_{R,L}^\pm$.

The main result of this work is the formulation of a more useful problem (P). Problem (P) will be defined with a function space V, which strengthens (1.4) and with a bilinear form β, which encodes a weaker version of (1.6), see (3.1). Theorem 3.3 provides the solvability of this problem and a stability estimate. The numerical results presented in Section 4 are obtained using problem (P).

1.2 Literature

An outgoing wave condition for homogeneous media was suggested by Sommerfeld in 1912, today it is the undoubted radiation condition for the full space problem. If, for numerical purpose, the domain is truncated, the radiation condition must be replaced by a condition at a finite distance. One of the ideas is to use a boundary condition that exploits a representation of the solution outside the truncated domain (integral representation or Dirichlet-to-Neumann map). Another idea is to introduce an absorbing layer that surrounds the truncated domain (perfectly matched layer technique).

Radiation conditions in periodic media. The two sketched ideas cannot easily be adapted to treat periodic media: Integral representations are not available and a non-reflecting boundary condition is not exact, since a non-homogeneous medium always reflects waves in part. The derivation of perfectly matched layers typically requires an explicit representation of propagating modes, which is not available in periodic media.

Outgoing wave conditions in periodic wave-guides have been introduced and analyzed e.g. in [12, 15]. Loosely speaking, a radiating solution is a function that consists, at large distances from the origin and up to small errors, of outgoing Bloch waves. The two contributions [12, 15] treat the (globally) periodic wave-guide problem and the periodic half-wave-guide problem, respectively, and they contain existence results that are based on a limiting absorption principle. A slightly different radiation condition for the locally periodic wave-guide was suggested in [24]. Regarding further results on limiting absorption principles we mention [19, 30].

Other conditions are the "modal radiation condition", formulated in Definition 2.4 of [3] and the "pole condition" of [17]. We mention [26] and the references therein for other approaches to radiation conditions.

Regarding the general treatment of waves in periodic media (e.g. in photonic crystals) we refer to [18, 21]. Regarding the tool of Bloch expansions and Bloch measures, we refer to [1].

Numerical treatment of radiation conditions. The numerical treatment of exact boundary conditions in an inhomogeneous material was considered in [10],

extending the approach of [19] to a material that is inhomogeneous in two directions. Their approach uses Dirichlet-to-Neumann maps that are defined by half-infinite wave guide problems. The authors provide an explanation why none of the classical approaches to implement outgoing wave conditions at finite distance (local radiation condition, perfectly matched layers, standard Dirichlet-to-Neumann maps) can easily be adapted to periodic media. We note that, just as in the contribution at hand, the analysis of [10] is restricted to the case with positive losses.

The method was developed further to a numerical scheme in [11]. The ideas were used in [9] to the study of line defects in a periodic photonic crystal; these defects have been analyzed also in [16] with the result that a line defect cannot support finite energy modes (bound states). For extensions of the numerical scheme to Robin type boundary conditions see [13].

Enriched finite elements. Our numerical method is a Galerkin method in which we use two different types of ansatz functions: Standard piecewise linear hat functions in the interior of the domain and Bloch waves in the radiation boxes. The approach is reminiscent of enriched finite element methods, see e.g. [20, 31].

Negative refraction. Photonic crystals can exhibit astonishing behavior – one of them is negative refraction. When a planar wave hits the interface between free space and photonic crystal, then one part of the wave is reflected, another part generates waves inside the photonic crystal. It has been observed that the waves in the crystal can travel in a direction that corresponds to negative refraction.

There are two explanations for this effect. The first one is based on a study of a homogenized equivalent medium that replaces the photonic crystal. This replacement provides a good approximation if the periodicity is small compared to the wave-length. We refer to Figure 4 for the numerical results of our method in this case. Indeed, the results show a good agreement between the solution with the periodic medium on the right and the solution with the homogenized medium. If the homogenized medium happens to have a negative index of refraction, then negative refraction is visible in the homogenized problem and also in the periodic problem (not the case in Figure 4). For the underlying idea we mention [28], for mathematical justifications we refer to [4, 5, 22, 23]. In [8, 29] the negative refraction effect is explained in the spirit of negative index materials.

The second explanation of the effect of negative refraction, observed and outlined in [25]. The main point of [25] is that negative refraction can occur between two materials with positive index (where no negative refraction occurs in the homogenization limit). The analysis is purely based on the study of the band structure of the left and right medium. Figure 5 illustrates this effect: The incoming wave from the left travels north-east. For the homogenized material in the right half (results of the bottom figure), the transmitted wave also travels north-east. In contrast, for wave-length and periodicity of comparable size (top figure), the transmitted wave travels south-east. Both [24] and the work at hand support the interpretation of [25]: Negative refraction is possible in positive index materials. We emphasize that we use here the same photonic crystal that was also used in [8] and [25]. This periodic medium does not have a negative effective index in the sense of homogenization.

2 Bloch expansion formalism and problem (P)

We have to fix the notations of the Bloch expansion formalism. The formalism allows us, on the one hand, to define the projections that have already been used in condition (1.4). On the other hand, we will be able to formulate the modified problem (P), which we suggest as a useful truncated problem.

We assume in the following that the medium is ε-periodic on the right and on the left. More precisely, for two Y_ε-periodic functions a_+ and a_-, we assume $a(x) = a_+(x)$ for $x_1 \geq \varepsilon R/2$ and $a(x) = a_-(x)$ for $x_1 \leq -\varepsilon R/2$. We work in two space dimensions, but the methods are not restricted to this case.

2.1 Bloch formalism

For $\varepsilon > 0$ let $Y_\varepsilon = \varepsilon(0,1)^2$ be the periodicity cell and let $H = \varepsilon K$ with $K \in \mathbb{N}$ be the height of the domain $\Omega = \mathbb{R} \times (0,H)_\sharp$. We use the finite index set $Q_K := \{0, \frac{1}{K}, \frac{2}{K}, \ldots, \frac{K-1}{K}\}$ and employ a Pre-Bloch expansion in the vertical direction: Any function $u \in L^2_{\mathrm{loc}}(\mathbb{R} \times (0,H); \mathbb{C})$ can be expanded in periodic functions with phase-shifts: There is a unique family of ε-periodic functions $\Phi_{j_2}(x_1, \cdot)$ such that, in the sense of $L^2_{\mathrm{loc}}(\mathbb{R} \times (0,H); \mathbb{C})$,

$$u(x_1, x_2) = \sum_{j_2 \in Q_K} \Phi_{j_2}(x_1, x_2)\, e^{2\pi \mathrm{i} j_2 x_2/\varepsilon}\,. \tag{2.1}$$

The analogous result holds when we expand a function $u \in L^2((0,\varepsilon L) \times (0,\varepsilon K); \mathbb{C})$ in both directions x_1 and x_2. In this case one obtains for $j = (j_1, j_2) \in Q_L \times Q_K$ functions $\Phi_j = \Phi_j(x_1, x_2)$ that are ε-periodic in both directions.

We regard the ε-periodic functions Φ_j for $j = (j_1, j_2)$ as maps $Y_\varepsilon \to \mathbb{C}$ and expand them in terms of eigenfunctions of the operator

$$\mathcal{L}_j^\pm := -\left(\nabla + 2\pi\mathrm{i} j/\varepsilon\right) \cdot \left(a_\pm(x)\left(\nabla + 2\pi\mathrm{i} j/\varepsilon\right)\right)\,, \tag{2.2}$$

which is defined on $H^1_\sharp(Y_\varepsilon; \mathbb{C})$. The definition of the operator $\mathcal{L}_j^\pm$ is motivated by the following fact: If $\Psi_j^\pm$ is an eigenfunction of $\mathcal{L}_j^\pm$ with eigenvalue $\mu_j^\pm$, then $\Psi_j^\pm e^{2\pi\mathrm{i} j\cdot x/\varepsilon}$ is a solution to the Helmholtz equation (1.1) with $a = a_\pm$ and $\omega^2 = \mu_j^\pm$ and $f = 0$.

Definition 2.1 (Bloch eigenfunctions)**.** *For $\varepsilon > 0$ and $j \in [0,1]^2$ we denote by $\left(\Psi_{j,m}^\pm\right)_{m\in\mathbb{N}_0}$ an orthogonal family of eigenfunctions to the symmetric operator $\mathcal{L}_j^\pm$, ordered to have $\mu_{m+1}^\pm(j) \geq \mu_m^\pm(j)$ for all $m \in \mathbb{N}_0$. We normalize with $⨍_{Y_\varepsilon} |\Psi_{j,m}^\pm|^2 = 1$.*

The subsequent lemma is a classical result on Bloch expansions, see e.g. [27].

Lemma 2.2 (Bloch expansion)**.** *For $L, K \in \mathbb{N}$ and $\varepsilon > 0$ we consider the rectangle $W = (0,\varepsilon L) \times (0,\varepsilon K)$ and $u \in L^2(W; \mathbb{C})$. For both eigenfunction families $(\Psi_{j,m}^+)_{j,m}$ and $(\Psi_{j,m}^-)_{j,m}$ the function u possesses a unique expansion with coefficients $\alpha_{j,m}^\pm \in \mathbb{C}$ and convergence in $L^2(W; \mathbb{C})$:*

$$u(x) = \sum_{j \in Q_L \times Q_K} \sum_{m=0}^{\infty} \alpha_{j,m}^\pm \Psi_{j,m}^\pm(x)\, e^{2\pi\mathrm{i} j\cdot x/\varepsilon}\,. \tag{2.3}$$

We use the index-set $I_{L,K} := \{(j,m)|j \in Q_L \times Q_K,\ m \in \mathbb{N}_0\}$ and multi-indices $\lambda = (j,m) \in I_{L,K}$, and define for $x \in (0,\varepsilon L) \times (0,\varepsilon K)$

$$U_\lambda^\pm(x) := \Psi_\lambda^\pm(x)\, e^{2\pi \mathrm{i} j\cdot x/\varepsilon}\,. \tag{2.4}$$

With this notation, (2.3) simplifies to

$$u(x) = \sum_{\lambda\in I_{L,K}} \alpha_\lambda^\pm U_\lambda^\pm(x)\,. \tag{2.5}$$

We note that the Bloch basis functions inherit orthogonality properties from the eigenfunctions $\Psi_{j,m}^\pm$. Given $L, K \in \mathbb{N}$, we calculate on $W = (0,\varepsilon L) \times (0,\varepsilon K)$ for $\lambda = (j,m)$ and $\tilde\lambda = (\tilde j, \tilde m)$, $\lambda, \tilde\lambda \in I_{L,K}$:

$$\int_W \bar U_\lambda^+(x) U_{\tilde\lambda}^+(x)\,dx = \int_W \Psi_\lambda^+(x)\Psi_{\tilde\lambda}^+(x) e^{2\pi\mathrm{i}(\tilde j - j)\cdot x/\varepsilon}\,dx = (\varepsilon^2 LK)\ \delta_{\lambda,\tilde\lambda}\,.$$

Indeed, for $j \neq \tilde j$, the expression vanishes by Lemma A.1 of [24]. For $j = \tilde j$ and $m \neq \tilde m$, the expression vanishes by orthogonality of the different eigenfunctions Ψ_λ^+ to one j. In the remaining case $\lambda = \tilde\lambda$, the statement is a consequence of the normalization of Ψ_λ^+. The same applies to $(U_\lambda^+)_\lambda$. Due to the $L^2(W)$-orthogonality, we have the Plancherel formula

$$\|u\|_{L^2(W)}^2 = \varepsilon^2 LK \sum_{\lambda\in I_{L,K}} |\alpha_\lambda^\pm|^2\,. \tag{2.6}$$

Poynting numbers, index sets and projections

We study a fixed index $\lambda \in I := \{\lambda = (j,m)|j \in [0,1]^2, m \in \mathbb{N}_0\}$. To the index λ we associate two Bloch waves, U_λ^+ and U_λ^- for the right domain and the left domain, respectively. The Bloch waves $U_\lambda^\pm$ can transport energy to the left or to the right; we now introduce the Poynting numbers $P_\lambda^\pm$ which indicate the direction of energy transport. The sign of P_λ^+ coincides with the sign of the first component of the group velocity, see Theorem 3 in [12] and the explanation in Section 3.1. of [24]. We set

$$P_\lambda^\pm := \mathrm{Im} \fint_{Y_\varepsilon} \bar U_\lambda^\pm(x)\, e_1 \cdot \left[a_\pm(x)\nabla U_\lambda^\pm(x)\right]\,dx\,. \tag{2.7}$$

Definition 2.3 (Projections)**.** *Let $u \in L^2(W;\mathbb{C})$ be a function on the rectangle $W = (0,\varepsilon L)\times(0,\varepsilon K)$ with the discrete Bloch expansion* (2.5)*. We define the projections $\Pi_{>0}^\pm$ onto right-going Bloch waves by*

$$\left(\Pi_{>0}^\pm u\right)(x) := \sum_{\substack{\lambda\in I_{L,K}\\ P_\lambda^\pm > 0}} \alpha_\lambda^\pm U_\lambda^\pm(x)\,. \tag{2.8}$$

Projections $\Pi_{<0}^\pm$ onto left-going Bloch waves are defined accordingly.

Sesquilinear forms $b^\pm$. We consider two functions $u \in L^2(W,\mathbb{C})$ and $v \in H^1(W,\mathbb{C})$ on the rectangle $W = (0,\varepsilon L)\times(0,\varepsilon K)$. Two energy-flux sesquilinear forms are defined by

$$b^\pm(u,v) := \fint_W \bar{u}(x)\, e_1 \cdot [a_\pm(x)\nabla v(x)]\; dx\,. \tag{2.9}$$

The connection to the Poynting number $P_\lambda^\pm$ of (2.7) is expressed by

$$P_\lambda^\pm = \operatorname{Im} b^\pm\left(U_\lambda^\pm, U_\lambda^\pm\right)\,. \tag{2.10}$$

The following lemma has been shown in [24] for $L = K$, the proof in the general case needs only notational changes.

Lemma 2.4 (Orthogonality property of $b^\pm$)**.** *Given $L, K \in \mathbb{N}$, let $\lambda, \tilde\lambda \in I_{L,K}$ be two indices with $\lambda = (j,m)$, $\tilde\lambda = (\tilde j, \tilde m)$ and $j \neq \tilde j$. Then the basis functions $U_\lambda^\pm$ and $U_{\tilde\lambda}^\pm$ of* (2.4) *satisfy*

$$b^\pm(U_\lambda^\pm, U_{\tilde\lambda}^\pm) = 0\,. \tag{2.11}$$

2.2 Problem (P)

We can now formulate the truncated problem (P). We propose this problem on a bounded domain as a replacement of the Helmholtz equation with a radiation condition.

Our aim is to modify problem (P_0), which was defined by equations (1.3)–(1.6). In problem (P) we keep equation (1.3). Equation (1.4) is strengthened, see (2.14) below. The continuity condition (1.5) is kept and the flux condition (1.6) is weakened, see (2.17).

The approximate problem is designed by choosing two index sets $I^+ \subset I_{L,K}$ and $I^- \subset I_{L,K}$. We recall that every element $\lambda \in I^\pm$ is of the form $\lambda = (j,m)$ with $j_1 \in Q_L \subset [0,1]$, $j_2 \in Q_K \subset [0,1]$, $m \in \mathbb{N}$. The index sets $I^\pm$ are chosen with the property

$$\lambda \in I^+ \Rightarrow P_\lambda^+ > 0, \quad \lambda \in I^- \Rightarrow P_\lambda^- < 0, \tag{2.12}$$

i.e. Bloch waves of the right radiation box travel to the right and Bloch waves of the left radiation box travel to the left. Moreover, in the numerics $I^\pm$ are finite. For given sets $I^\pm$ we define the space

$$X^\pm := \operatorname{span}\{U_\lambda^\pm \mid \lambda \in I^\pm\}\,. \tag{2.13}$$

In order to approximate the Helmholtz equation on the unbounded domain we first choose $R, L, \delta > 0$, and the two index sets $I^\pm$. Given these parameters, the aim is to find $u : \Omega_{R+L} \to \mathbb{C}$ that satisfies the following four conditions: (i) The Helmholtz equation (1.3) on Ω_R. (ii) The radiation condition (1.4) in the strengthened form

$$\{u\}_{R,L}^\pm \in X^\pm\,. \tag{2.14}$$

We recall that, when $I^\pm$ consists only of indices of outgoing waves, the projections (1.4) onto incoming waves automatically vanish. (iii) The weak continuity condition (1.5). (iv) A continuity condition that replaces (1.6); we obtain this condition as the natural interface condition in a variational formulation of the problem.

Problem (P) will be made precise in Definition 2.5 below. Essentially, the aim is to find u that satisfies (i)–(iv).

The variational formulation

In order to impose conditions (ii) and (iii), we seek u in the infinite dimensional function space

$$V := \left\{ u \in H^1(\Omega_{R+L}) \,\middle|\, u \text{ vertically periodic},\ \{u\}^+_{R,L} \in X^+, \{u\}^-_{R,L} \in X^- \right\}. \tag{2.15}$$

Note that V depends on the choice of the index sets $I^\pm$.

We now formulate (i) (the Helmholtz equation (1.3)) in a weak form, and, at the same time, encode the flux condition (iv). In order to make integration by parts possible, we introduce the special cut-off function $\vartheta : \mathbb{R} \to [0,1]$, defined by

$$\vartheta(\xi) := \begin{cases} 0 & \text{for } |\xi| \geq \varepsilon(R+L), \\ 1 & \text{for } |\xi| \leq \varepsilon R, \\ (\varepsilon(R+L) - |\xi|)/(\varepsilon L) & \text{else,} \end{cases}$$

compare Figure 2. We regard ϑ also as a function on two-dimensional domains such as Ω_{R+L} by setting $\vartheta(x_1, x_2) = \vartheta(x_1)$.

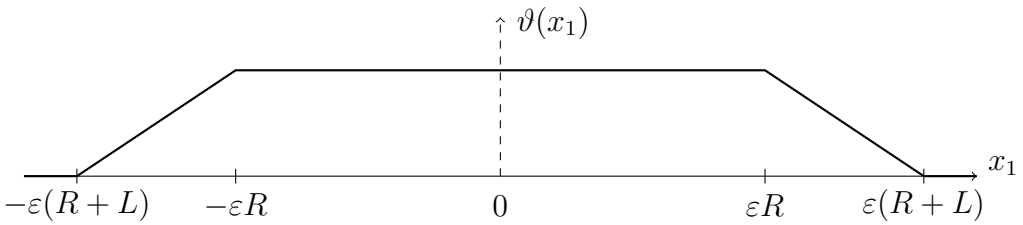

Figure 2: The cut-off function ϑ

In order to motivate the central definition of this article, we take the complex conjugate of the Helmholtz equation (1.3) and multiply with the product $v\,\vartheta$, where $v \in V$ is arbitrary. We obtain

$$\int_{\Omega_{R+L}} a \nabla \bar{u} \cdot \nabla(v\,\vartheta) - \int_{\Omega_{R+L}} (1 - \mathrm{i}\delta \mathbf{1}_{\Omega_R})\, \omega^2 \bar{u}\, v\, \vartheta = \int_{\Omega_{R+L}} \bar{f}\, v\, \vartheta\,.$$

The gradient of ϑ can be expressed explicitly as $\nabla\vartheta = -(\varepsilon L)^{-1} e_1$ on $W^+_{R,L}$, $\nabla\vartheta = (\varepsilon L)^{-1} e_1$ on $W^-_{R,L}$, and $\nabla\vartheta = 0$ on Ω_R. We use the above relation to define an approximate problem.

Definition 2.5 (Problem (P))**.** *Given $R, L, \delta > 0$, the index sets $I^\pm$, and $f \in L^2(\Omega)$ with support in Ω_R, a function $u \in V$ is called a solution to problem (P) if*

$$\begin{aligned} \beta(u,v) := &\int_{\Omega_{R+L}} a \nabla \bar{u} \cdot \nabla v\, \vartheta - \int_{\Omega_{R+L}} (1 - \mathrm{i}\delta \mathbf{1}_{\Omega_R})\, \omega^2 \bar{u}\, v\, \vartheta \\ &- \frac{1}{\varepsilon L} \int_{W^+_{R,L}} a \nabla \bar{u} \cdot e_1\, v + \frac{1}{\varepsilon L} \int_{W^-_{R,L}} a \nabla \bar{u} \cdot e_1\, v = \int_{\Omega_R} \bar{f}\, v \end{aligned} \tag{2.16}$$

holds for every $v \in V$.

Remark 2.6. *Problem (P) is formally equivalent to the Helmholtz equation* (1.3). *More precisely, the following holds:*

Let u be a solution (P). Then u solves the Helmholtz equation (1.3) *on Ω_R.*

Let $u \in H^1(\Omega_{R+L})$ be a solution of the Helmholtz equation (1.3) *on Ω_{R+L} with δ replaced by $\delta \mathbf{1}_{\Omega_R}$ and with the source f supported in Ω_R. Then u satisfies* (2.16) *(but not necessarily $u \in V$).*

Proof. Regarding the first statement, we consider an arbitrary test-function $v \in C_c^\infty(\Omega_R)$. Then $v\,\vartheta = v$ and $\nabla v\,\vartheta = \nabla v$, integrals over $W_{R,L}^\pm$ vanish. Therefore (2.16) is nothing but the weak formulation of (1.3).

To verify the second statement, it suffices to take the conjugate complex of (1.3), to multiply with $v\,\vartheta$ and to integrate. No boundary terms appear in the integration by parts since ϑ vanishes for $x_1 = \pm(R+L)$. □

The coupling condition in a special case. Let us investigate solutions to (P) in the case $\delta = 0$, assuming that $X^\pm$ is spanned by Bloch waves $U_\lambda^\pm$ that have exactly the eigenvalue ω^2. We can integrate by parts in (2.16) and obtain

$$-\int_{\Omega_{R+L}} \nabla\cdot(a\nabla\bar u)v\,\vartheta - \int_{\Omega_{R+L}} \omega^2 \bar u\, v\,\vartheta \\ -\int_{\Gamma_R^+} [e_1\cdot a\nabla\bar u]_{\Gamma_R^+}\, v + \int_{\Gamma_R^-} [e_1\cdot a\nabla\bar u]_{\Gamma_R^-}\, v = \int_{\Omega_R} \bar f\, v\,.$$

The function u solves the Helmholtz equation in Ω_R by Remark 2.6. On the other hand, as a linear combination of solutions, u solves the Helmholtz equation also in $W_{R,L}^\pm$. This implies that the first two integrals cancel with the right hand side. Since v was arbitrary in V, we have

$$\int_{\Gamma_R^\pm} [e_1\cdot a\nabla u]_{\Gamma_R^\pm}\, U_\lambda^\pm = 0 \quad \text{for every } \; U_\lambda^\pm \in X^\pm\,. \tag{2.17}$$

In this sense, problem (P) implements a weak flux condition that replaces (1.6).

3 Existence result

Problem (P) of Definition 2.5 reads: Find $u \in V$ that satisfies

$$\beta(u,v) = \int_{\Omega_R} \bar f\, v \qquad \forall v \in V\,. \tag{3.1}$$

We will derive a coercivity result for the form β and obtain, as a corollary, an existence result for problem (P). The coercivity result will be based on the following assumptions.

Assumption 3.1. *We introduce the following assumptions on the index sets $I^\pm$ and the corresponding spaces $X^\pm$.*

(A1) Positive speed: There exists a positive number $c_0 > 0$ such that, for every λ with $U_\lambda^\pm \in X^\pm$, there holds

$$\pm P_\lambda^\pm \geq c_0\,. \tag{3.2}$$

(A2) For every pair of indices $\lambda = (j, m), \tilde{\lambda} = (\tilde{j}, \tilde{m}) \in I^{\pm}$ the wave numbers are different: $j \neq \tilde{j}$.

(A3) Regularity: For some constant $C_0 > 0$ and every $u \in X^{\pm}$ holds

$$\|u\|^2_{H^1(W)} \leq C_0 \|u\|^2_{L^2(W)} \,. \tag{3.3}$$

Remark 3.2. *On Assumption 3.1. (i) Assumption (A2) is only used to exploit $b^{\pm}(U^{\pm}_{\lambda}, U^{\pm}_{\tilde{\lambda}}) = 0$ for $\tilde{\lambda} \neq \lambda$. The assumption is not essential for the numerical scheme. (ii) If Assumption (A2) is satisfied, then the sets I^+ and I^- are necessarily finite and the spaces $X^{\pm}$ are finite dimensional. (iii) When I^+ and I^- are finite sets, then (A3) is automatically satisfied since all functions $U^{\pm}_{\lambda}$ possess H^1-regularity. Under the same assumption, (A1) is satisfied if and only if no wave $U^{\pm}_{\lambda}$ is used in $X^{\pm}$, which travels in vertical direction.*

Theorem 3.3 (Existence result for problem (P))**.** *Let R, L, δ be positive parameters and let $f \in L^2(\Omega)$ be a function with support in Ω_R. Let the coefficient function $a \in L^{\infty}(\Omega; \mathbb{R})$ be bounded from below by $a_0 > 0$ and identical to Y_{ε}-periodic functions $a_{\pm}$ for $\pm x_1 > \varepsilon R/2$. Let the index sets $I^{\pm}$ satisfy properties (A1)–(A3) of Assumption 3.1 with constants $c_0, C_0 > 0$. Then problem (P) of Definition 2.5 has a unique solution u. For a constant $C = C(R, L, a_0, \delta, c_0, C_0)$ we have the stability estimate*

$$\|u\|_{H^1(\Omega_{R+L})} \leq C \|f\|_{L^2(\Omega_R)} \,. \tag{3.4}$$

We derive the above theorem with a constant C that satisfies $C \sim \delta^{-1}$ for small δ. The numerical experiments show a much better behavior of the solution u: The scheme has good convergence properties even for $\delta = 0$.

Proof of Theorem 3.3. The aim on the next pages is to derive, for two numbers $\sigma, \gamma > 0$, a coercivity estimate of the form

$$\operatorname{Im} \beta(u, u) + \sigma\delta \operatorname{Re} \beta(u, u) \geq \gamma \|u\|^2_{H^1(\Omega_{R+L})} \,. \tag{3.5}$$

We obtain this result as relation (3.13) in Proposition 3.6.

The Lax-Milgram Lemma implies the existence statement of Theorem 3.3. We note that the Lax-Milgram lemma in complex Hilbert spaces is applicable for sesquilinear forms that satisfy a coercivity estimate of the form (3.5). We refer to [2] for a proof of the Lax-Milgram Lemma that works with the coercivity assumption $|\beta(u, u)| \geq \gamma \|u\|^2_{H^1}$, which is implied by (3.5).

Let us recall here the main point of the proof, which is the derivation of estimate (3.4) for solutions of (3.1): Using $v = u \in V$ as a test-vector in (3.1) and exploiting (3.5) yields

$$\begin{aligned} \gamma \|u\|^2_{H^1(\Omega_{R+L})} &\leq \operatorname{Im} \beta(u, u) + \sigma\delta \operatorname{Re} \beta(u, u) \leq (1 + \sigma\delta) |\beta(u, u)| \\ &\leq (1 + \sigma\delta) \left| \int_{\Omega_R} \bar{f}\, u \right| \leq (1 + \sigma\delta) \|f\|_{L^2(\Omega_R)} \|u\|_{L^2(\Omega_R)} \,. \end{aligned}$$

This provides (3.4) with the constant $C = (1 + \sigma\delta)\gamma^{-1}$. □

3.1 Coercivity in L^2

The main feature of the bilinear form β is the positivity of the imaginary part. Moreover, the imaginary part controls certain norms of the argument.

Lemma 3.4 (L^2-coercivity)**.** *Let the index sets $I^\pm$ satisfy the outgoing wave property* (2.12)*. Then the sesquilinear form β of Definition 2.5 satisfies the following L^2-coercivity estimate:*

$$\operatorname{Im} \beta(u,u) \geq \delta\omega^2 \|u\|^2_{L^2(\Omega_R)} \qquad \forall u \in V\,. \tag{3.6}$$

Let additionally the positive speed property (3.2) *be satisfied in $X^\pm$ with the constant $c_0 > 0$. Then we have the stronger estimate*

$$\operatorname{Im} \beta(u,u) \geq \delta\omega^2 \|u\|^2_{L^2(\Omega_R)} + \frac{c_0}{\varepsilon L} \left(\|u\|^2_{L^2(W^+_{R,L})} + \|u\|^2_{L^2(W^-_{R,L})} \right). \tag{3.7}$$

Proof. Let $u \in V$ be arbitrary. By definition of the space V, the function u can be expanded in Bloch waves in the two rectangles $W^\pm_{R,L}$. We write the shifted functions as

$$\{u\}^+_{R,L} = \sum_{\lambda \in I^+} \alpha^+_\lambda U^+_\lambda\,, \qquad \{u\}^-_{R,L} = \sum_{\lambda \in I^-} \alpha^-_\lambda U^+_\lambda\,. \tag{3.8}$$

With β from (2.16) we now calculate $\beta(u,u)$. The integrals over $W^\pm_{R,L}$ can be expressed with the sesquilinear forms $b^\pm$ from (2.9). The orthogonality property of Lemma 2.4 allows to calculate

$$\begin{aligned}
\beta(u,u) &= \int_{\Omega_{R+L}} a|\nabla u|^2\,\vartheta - \int_{\Omega_{R+L}} (1 - \mathrm{i}\delta \mathbf{1}_{\Omega_R})\,\omega^2 |u|^2 \vartheta \\
&\quad - \varepsilon K\, \overline{b^+} \left(\{u\}^+_{R,L}, \{u\}^+_{R,L} \right) + \varepsilon K\, \overline{b^-} \left(\{u\}^-_{R,L}, \{u\}^-_{R,L} \right) \\
&= \int_{\Omega_{R+L}} a|\nabla u|^2\,\vartheta - \int_{\Omega_{R+L}} (1 - \mathrm{i}\delta \mathbf{1}_{\Omega_R})\,\omega^2 |u|^2 \vartheta \\
&\quad - \varepsilon K \sum_{\lambda \in I^+} |\alpha^+_\lambda|^2\, \overline{b^+}(U^+_\lambda, U^+_\lambda) + \varepsilon K \sum_{\lambda \in I^-} |\alpha^-_\lambda|^2\, \overline{b^-}(U^-_\lambda, U^-_\lambda)\,.
\end{aligned}$$

Taking the imaginary part and using the definition of $P^\pm$ from (2.10), we obtain

$$\operatorname{Im} \beta(u,u) = \int_{\Omega_R} \delta\,\omega^2 |u|^2 + \varepsilon K \sum_{\lambda \in I^+} |\alpha^+_\lambda|^2 P^+_\lambda - \varepsilon K \sum_{\lambda \in I^-} |\alpha^-_\lambda|^2 P^-_\lambda\,. \tag{3.9}$$

Non-negativity of P^+_λ for $\lambda \in I^+$ and non-positivity of P^-_λ for $\lambda \in I^-$ implies the lower bound (3.6).

Estimate (3.7). In the case that the positive speed property is satisfied, the box integrals yield a strictly positive contribution. Inserting (3.2) into (3.9) we find

$$\begin{aligned}
\operatorname{Im} \beta(u,u) &\geq \int_{\Omega_R} \delta\,\omega^2 |u|^2 + c_0 \varepsilon K \left(\sum_{\lambda \in I^+} |\alpha^+_\lambda|^2 + \sum_{\lambda \in I^-} |\alpha^-_\lambda|^2 \right) \\
&\geq \int_{\Omega_R} \delta\,\omega^2 |u|^2 + \frac{c_0}{\varepsilon L} \left(\int_{W^+_{R,L}} |u|^2 + \int_{W^-_{R,L}} |u|^2 \right),
\end{aligned} \tag{3.10}$$

where we used the Plancherel formula (2.6) in the last line. This yields (3.7). □

Remark 3.5. *(i) The $L^2(\Omega_R)$ coercivity of Lemma 3.4 is not sufficient for an existence result since the sesquilinear form β is defined on $H^1(\Omega_{R+L})$.*

(ii) The lower bound in (3.6) depends on δ. This fact is discouraging when one seeks to perform a limiting absorption principle, which needs estimates that are uniform in δ. By contrast, considering only the norm of the solution in the radiating boxes $W^{\pm}_{R,L}$, the bound in (3.7) is independent of δ. This δ-independent bound seems to be the reason for the numerically observed stability of problem (P): The scheme works well even for $\delta = 0$.

3.2 Coercivity in H^1

We turn now to the coercivity estimate that corresponds to the chosen function space. The two assumptions in (3.11) and (3.12) essentially demand the smallness of σ in comparison to 1 and to c_0/δ.

Proposition 3.6 ($H^1(\Omega_{R+L})$-coercivity)**.** *Let the index sets $I^{\pm}$ satisfy properties (A1)–(A3) of Assumption 3.1 with constants $c_0, C_0 > 0$. Let $\sigma > 0$ be small enough to satisfy the two properties*

$$\sigma \leq \min\left\{\frac{1}{2}, \frac{c_0}{4\varepsilon L \delta \omega^2}\right\}, \tag{3.11}$$

$$2\sigma\delta \ \left|\operatorname{Re} b^{\pm}(U^{\pm}_{\lambda}, U^{\pm}_{\lambda})\right| \leq \operatorname{Im} b^{\pm}(U^{\pm}_{\lambda}, U^{\pm}_{\lambda}) \qquad \forall \lambda \text{ with } U^{\pm}_{\lambda} \in X^{\pm}. \tag{3.12}$$

Then there exists $\gamma = \gamma(c_0, \delta, \sigma, \omega, a_0) > 0$ such that for every $u \in V$ holds

$$\operatorname{Im}\beta(u,u) + \sigma\delta \ \operatorname{Re}\beta(u,u) \geq \gamma \|u\|^2_{H^1(\Omega_{R+L})}. \tag{3.13}$$

Proof. Relation (3.7) of Lemma 3.4 together with (3.9) provides the following lower bound for the imaginary part of $\beta(u,u)$:

$$\begin{aligned}\operatorname{Im}\beta(u,u) \geq{}& \delta\omega^2 \|u\|^2_{L^2(\Omega_R)} + \frac{c_0}{2\varepsilon L}\left(\|u\|^2_{L^2(W^+_{R,L})} + \|u\|^2_{L^2(W^-_{R,L})}\right) \\ &+ \frac{\varepsilon K}{2}\sum_{\lambda\in I^+} |\alpha^+_\lambda|^2 P^+_\lambda - \frac{\varepsilon K}{2}\sum_{\lambda\in I^-} |\alpha^-_\lambda|^2 P^-_\lambda .\end{aligned} \tag{3.14}$$

We now evaluate the real part of $\beta(u,u)$ from its definition in (2.16). After a multiplication with the factor $\sigma\delta$ we find, with the orthogonality (2.11),

$$\begin{aligned}\sigma\delta \ \operatorname{Re}\beta(u,u) = {}& \sigma\delta \int_{\Omega_{R+L}} a|\nabla u|^2 \,\vartheta - \sigma\delta \int_{\Omega_{R+L}} \omega^2 |u|^2 \vartheta \\ &- \sigma\delta\,\varepsilon K \sum_{\lambda\in I^+} |\alpha^+_\lambda|^2 \operatorname{Re} b^+(U^+_\lambda, U^+_\lambda) + \sigma\delta\,\varepsilon K \sum_{\lambda\in I^-} |\alpha^-_\lambda|^2 \operatorname{Re} b^-(U^-_\lambda, U^-_\lambda).\end{aligned} \tag{3.15}$$

Due to assumption (3.12) on σ, the two sums in (3.15) are smaller in absolute value than the two sums in (3.14). Due to assumption (3.11) on σ, the second integral in (3.15) is bounded in absolute value by the half of the first two contributions on the right hand side of (3.14). We therefore obtain

$$\begin{aligned}\operatorname{Im}\beta(u,u) + \sigma\delta \ \operatorname{Re}\beta(u,u) \geq{}& \frac{\delta\omega^2}{2}\|u\|^2_{L^2(\Omega_R)} + \frac{c_0}{4\varepsilon L}\left(\|u\|^2_{L^2(W^+_{R,L})} + \|u\|^2_{L^2(W^-_{R,L})}\right) \\ &+ \sigma\delta a_0 \int_{\Omega_{R+L}} |\nabla u|^2 \,\vartheta ,\end{aligned}$$

where $a \geq a_0$ was used. The inverse estimate (3.3) implies that the right hand side controls the squared $H^1(\Omega_{R+L})$-norm. We thus arrive at (3.13). □

Remark 3.7. *An inspection of the assumptions on σ shows that the coercivity constant γ has the properties $\gamma \sim \delta$ for small $\delta > 0$ and $\gamma \sim \sigma \sim c_0$ for small $c_0 > 0$.*

4 Numerical method and examples

4.1 Numerical method

Finite element discretization of problem (P)

Our aim is to approximate problem (P) with a finite element method (FEM), using an enriched, problem adapted set of basis functions. Once a finite dimensional subspace V_h of V is defined with basis functions, we have obtained in a natural way a discretization of problem (P). Our construction uses piecewise linear hat functions on a triangular mesh. More precisely, the space V_h is spanned by standard (piecewise linear) hat functions in Ω_R and by (approximation of) Bloch waves in the radiation boxes. We use Bloch waves U_λ^+ with a positive Poynting number in the radiation box $W_{R,L}^+$ and U_λ^- with a negative Poynting number in the box $W_{R,L}^-$. The Bloch waves themselves are computed with piecewise linear hat functions.

Choice of a regular grid. We use a (uniform) triangulation mesh with right angled triangles on $\overline{\Omega_{R+L}}$. The fineness parameters $h_1 > 0$ and $h_2 > 0$ denote the lengths of the triangle legs in the x_1 and x_2 directions respectively. The grid points $x^{(k)} \in \overline{\Omega_{R+L}}$, $k = 1, \ldots, N_h$ are enumerated so that

$$x^{(k)} \in \begin{cases} (-\varepsilon R, \varepsilon R) \times [0, \varepsilon K) & \text{for } k = 1, \ldots, N_0, \\ \overline{W_{R,L}^+} & \text{for } k = N_0 + 1, \ldots, N_0 + N_W, \\ \overline{W_{R,L}^-} & \text{for } k = N_0 + N_W + 1, \ldots, N_0 + 2N_W = N_h. \end{cases}$$

Hat functions. To the grid we assign the standard piecewise linear hat functions $\phi_k, k = 1, \ldots, N_h$ with $\phi_k(x^{(l)}) = \delta_{k,l}$ for $k, l = 1, \ldots, N_h$. To impose vertical periodicity in Ω_R, each hat function ϕ_k with $x^{(k)} \in [-\varepsilon(R+L), \varepsilon(R+L)] \times \{0\}$ (i.e. a lower boundary point) consists of the hat function half corresponding to $x^{(k)}$ and the hat function half corresponding to the artificial grid point $(x_1^{(k)}, x_2^{(k)} + \varepsilon K)$. These hat functions (and, hence, any linear combination thereof) are periodic in the vertical direction.

Bloch waves. Next, we define the Bloch wave basis functions. For each selected wave vector j we first solve the eigenvalue problems $\mathcal{L}_j^\pm \Psi_j^\pm = \mu^\pm(j) \Psi_j^\pm$ on the cube Y_ε with periodic boundary conditions. The FEM-solutions to these problems are denoted $\Psi_{j,m}^{\pm,h}$, $m \in \mathbb{N}$.

For each m in an appropriately chosen subset of $\mathbb{N}$ we extend the solution by periodicity onto the radiation box $\overline{W_{R,L}^\pm}$ and use (2.4) to define $U_\lambda^{\pm,h}$ (recall that $\lambda = (j, m)$). Each Bloch wave $U_\lambda^{\pm,h}$ is extended by zero to all grid points outside $\overline{W_{R,L}^\pm}$. Our selected set of indices λ is denoted by $I^{\pm,h}$ and is specified below.

The resulting Bloch waves can be written, for each $\lambda_i \in I^{\pm,h}$, as

$$U^{+,h}_{\lambda_i}(x) = \sum_{k=N_0+1}^{N_0+N_W} \kappa_k^{+,i}\phi_k(x), \quad U^{-,h}_{\lambda_i}(x) = \sum_{k=N_0+N_W+1}^{N_h} \kappa_k^{-,i}\phi_k(x)\,, \tag{4.1}$$

with coefficients $\kappa_k^{\pm,i} \in \mathbb{C}$ for all i,k. We emphasize that the functions $U^{\pm,h}_{\lambda_i}$ are continuous on $\overline{\Omega_{R+L}}$ for all i. On the other hand, they are concentrated in the radiation boxes in the sense that $U^{+,h}_{\lambda_i}(x^{(k)}) = 0$ for $x_1^{(k)} < \varepsilon R$, $U^{-,h}_{\lambda_i}(x^{(k)}) = 0$ for $x_1^{(k)} > -\varepsilon R$.

The sets $I^{\pm,h}$ are discrete analogs of $I^{\pm}$ satisfying (A1)–(A3) in Assumption 3.1. However, in contrast to $I^{\pm}$ we choose for the numerics the $j-$domain to be $\mathbb{B} := \left(-\frac{1}{2}, \frac{1}{2}\right]^2$, such that $\frac{2\pi}{\varepsilon}\mathbb{B}$ is the standard Brillouin zone corresponding to the periodicity cell Y_ε. This symmetric choice has the advantage that the band structure plots clearly show the conical shape in the case of homogeneous media. The set Q_K from Section 2 (defined to ensure the vertical εK-periodicity of the solution in $W^{\pm}_{R,L}$) needs to be modified to

$$Q'_K := \begin{cases} \{-\frac{K-2}{2K}, -\frac{K-4}{2K}, \dots, \frac{1}{2}\}, & \text{for } K \in 2\mathbb{N}, \\ \{-\frac{K-1}{2K}, -\frac{K-3}{2K}, \dots, \frac{K-1}{2K}\}, & \text{for } K \in 2\mathbb{N}+1. \end{cases}$$

The Poynting numbers $P^{\pm}_{\lambda}$ are computed via a numerical quadrature of (2.7) in the piecewise linear finite element space.

Approximation of the space V. Assuming for simplicity that the number of Bloch basis functions is the same in both radiation boxes, $|I^{+,h}| = |I^{-,h}| =: N_{\mathrm{Bl}} \in \mathbb{N}$, we can now define the finite dimensional space as

$$V_h := \operatorname{span}\{\psi_1, \dots, \psi_{N_0+2N_{\mathrm{Bl}}}\}, \tag{4.2}$$

where

$$\psi_k := \begin{cases} \phi_k & \text{for } k = 1, \dots N_0, \\ U^{+,h}_{\lambda_i} \text{ with } \lambda_i \in I^{+,h} & \text{for } k = N_0 + i, i = 1, \dots, N_{\mathrm{Bl}}, \\ U^{-,h}_{\lambda_i} \text{ with } \lambda_i \in I^{-,h} & \text{for } k = N_0 + N_{\mathrm{Bl}} + i, i = 1, \dots, N_{\mathrm{Bl}}. \end{cases}$$

Discretization of problem (P). The finite dimensional subspace $V_h \subset V$ defines a discrete problem (P). The complex conjugate of (2.16) can be written with matrices and coordinate vectors as

$$\mathbf{A}\vec{U} - \mathbf{B}\vec{U} - \omega^2\mathbf{M}^{(\delta)}\vec{U} = \vec{F}\,.$$

Here $\vec{U} \in \mathbb{C}^{N_0+2N_{\mathrm{Bl}}}$ is the unknown coordinate vector and the matrix entries are, for each $k,l = 1, \dots, N_0 + 2N_{\mathrm{Bl}}$,

$$\begin{aligned} \mathbf{A}_{k,l} &= \textstyle\int_{\Omega_{R+L}} a\vartheta\nabla\overline{\psi_k}\cdot\nabla\psi_l, & \mathbf{B}_{k,l} &= \frac{1}{\varepsilon L}\left(\int_{W^+_{R,L}} a\overline{\psi_k}e_1\cdot\nabla\psi_l - \int_{W^-_{R,L}} a\overline{\psi_k}e_1\cdot\nabla\psi_l\right), \\ \mathbf{M}^{(\delta)}_{k,l} &= (1+\mathrm{i}\delta\mathbf{1}_{\Omega_R})\textstyle\int_{\Omega_{R+L}}\overline{\psi_k}\psi_l, & F_k &= \textstyle\int_{\Omega_R} f\overline{\psi_k}. \end{aligned}$$

Due to the representation (4.1), all integrals involving the Bloch waves $U^{\pm,h}_{\lambda_i}$ can be evaluated using solely integrals of hat functions ϕ_k.

Numerical implementation caveats

Choice of the Bloch indices $I^{\pm,h}$. A suitable choice of the index sets $I^{\pm,h}$ is crucial for an efficient and accurate numerical scheme. A direct analog of $I^{\pm}$ satisfying $I^{\pm} \subset I_{L,K}$ and assumptions (A1)–(A2) can be built by the following procedure. First, for each $j \in Q'_L \times Q'_K$ one solves the Bloch eigenvalue problems $\mathcal{L}_j^{\pm}\Psi_j^{\pm} = \mu^{\pm}(j)\Psi_j^{\pm}$ in the FEM-approximation. For each j one keeps only the eigenvalue $\mu_m^{\pm}(j)$ closest to ω^2, which selects a natural number m for every vector j. Subsequently, one filters out eigenvalues $\mu_m^{+}(j)$ with a non-positive Poynting number of the Bloch wave and eigenvalues $\mu_m^{-}(j)$ with a non-negative Poynting number of the Bloch wave. The remaining pairs (j, m) define the sets $I^{\pm,h}$.

Numerical tests have shown that this approach works, but more accurate results are obtained when the horizontal L-periodicity requirement (i.e. $j_1 \in Q'_L$) is dropped. We take the liberty to choose points $(j, m) \in I^{\pm,h}$ so that the frequency level ω^2 is better realized: $|\omega^2 - \mu_m^{\pm}(j)|$ is minimized.

In practice, we first solve the eigenvalue problems $\mathcal{L}_j^{\pm}\Psi_j^{\pm} = \mu^{\pm}(j)\Psi_j^{\pm}$ in the FEM-approximation for all j (with $j_2 \in Q'_K$) on a selected j_1-mesh of $(-1/2, 1/2]$. For each j we save only the eigenvalue $\mu_m^{\pm}(j)$ closest to ω^2. Subsequently, for each $j_2 \in Q'_K$ we search for intersections of the line $\left(-\frac{1}{2}, \frac{1}{2}\right] \times \{j_2\}$ with the level set of the band structure at ω^2. Such intersections can occur for more eigenvalue families $\mu_m^{\pm}, m \in \mathbb{N}$. For each such family $\mu_m^{\pm}$ the intersections are found by an interpolation producing an approximation of the j_1-coordinates at which $\mu_m^{\pm}(j_1, j_2) = \omega^2$. The resulting pair $(m, (j_1, j_2))$ is then included in the set $I^{\pm,h}$ if the Poynting number of the Bloch wave $U_{(j,m)}^{\pm,h}$ has the appropriate sign. Including these intersection points in $I^{\pm,h}$ leads to the same accuracy of the calculations with a much smaller number N_{Bl}.

Orthogonalization of the Bloch waves $U_{\lambda_i}^{\pm,h}$ with $\lambda_i \in I^{\pm,h}$. The index set $I^{\pm,h}$ selected by the above procedure typically contains j-points lying no further than $\frac{\pi}{\varepsilon K}$ apart. This separation is small for K large and the corresponding Bloch waves $U_{\lambda_i}^{+,h}, \lambda_i \in I^{+,h}$ are similar if they belong to the same m. In order to keep the condition number of $\mathbf{A}$ small, we L^2-orthonormalize the set $U_{\lambda_i}^{+,h}, \lambda_i \in I^{+,h}$ via the modified Gram-Schmidt procedure. The superscript "$-$" is treated analogously.

Scattering problem with an incoming wave. When studying scattering problems with an incoming field $u^{(\mathrm{in})}$ supported on $x_1 < 0$, we use the following method to transform $u^{(\mathrm{in})}$ into the inhomogeneity f (without changing f on $x_1 \geq 0$). We set

$$u_\theta := u - u^{(\mathrm{in})}\theta \quad \text{with } \theta(x_1, x_2) = \theta(x_1) = \begin{cases} 1, & x_1 < -\varepsilon R \\ 1 - \tanh(d(x_1 + \frac{\varepsilon R}{2})), & x_1 \in [-\varepsilon R, 0) \\ 0, & x_1 \geq 0, \end{cases}$$

where d is sufficiently large to ensure that θ is close to zero at $x_1 = 0$. This leads to the transformed problem

$$-\nabla \cdot (a\nabla u_\theta) - \omega^2(1 + \mathrm{i}\delta)u_\theta = \tilde{f}, \quad \tilde{f} := f + 2a\nabla u^{(\mathrm{in})} \cdot \nabla\theta + u^{(\mathrm{in})}a\Delta\theta\,, \qquad (4.3)$$

which we treat exactly as described above.

4.2 Numerical results I: Comparison with homogenization

In our first numerical example we consider the interface between a homogenous and a periodic material and study a single incoming plane wave $u^{(\mathrm{in})} = e^{\mathrm{i}j^{(\mathrm{in})}\cdot x}$, $j^{(\mathrm{in})} \in \mathbb{R}^2$. We use the method developed above to calculate an approximate solution $u = u_\theta + u^{(\mathrm{in})}$, where u_θ solves (4.3). We compare this solution u of the original problem with the solution u_{hom} of the interface problem with a homogenized material on the right.

We choose $\varepsilon = 1$, $R = 15$, $L = 6$ and $H = 14$ and a discretization given by $h_1 = 0.05$ and $h_2 \approx 0.0526$. We use $N_{\mathrm{Bl}} = 4$ Bloch waves in each radiation box. The absorption constant is set to $\delta = 10^{-4}$. The heterogeneous material is described by the constant 1 ("air") on $x_1 < 0$ and a periodic array of discs on $x_1 \geq 0$. We choose the same structure as in [25], i.e.

$$a(x) = \begin{cases} 1, & x_1 < 0 \\ a_+(x), & x_1 \geq 0 \end{cases} \tag{4.4}$$

with

$$a_+(x) := \begin{cases} \frac{1}{12}, & \mathrm{dist}(x, \{(\frac{1}{2}, 0), (0, \frac{1}{2}), (\frac{1}{2}, 1), (1, \frac{1}{2})\}) < \frac{1}{\sqrt{2}} 0.35 \\ 1 & \text{otherwise} \end{cases} \tag{4.5}$$

for $x \in Y_\varepsilon$ and $a_+(x) = a_+(x + \varepsilon e_j)$, $j = 1, 2$ for all $x \in \mathbb{R}^2$.

The incoming wave $u^{(\mathrm{in})}(x) = e^{\mathrm{i}j^{(\mathrm{in})}\cdot x}$ has to satisfy $\omega^2 = |j^{(\mathrm{in})}|^2$ since $a \equiv 1$ on $x_1 < 0$.

For $\varepsilon \to 0$ (or, equivalently, for incoming waves of large period) the problem on $x_1 \geq 0$ can be approximated by the homogenized equation [6, 7]

$$\begin{aligned} &- a_* \Delta u_{\mathrm{hom}} = \omega^2 u_{\mathrm{hom}} \,, \\ &a_* = \frac{1}{2} \left(\frac{\varepsilon}{2\pi}\right)^2 \partial_{j_1}^2 \mu_0^+(0) = \fint_{Y_\varepsilon} a_+(x) \left[1 - \frac{\mathrm{i}}{2} \left(\partial_{x_1}\partial_{k_2}\psi_0^+(x) + \partial_{x_2}\partial_{k_1}\psi_0^+(x)\right)\right] dx \,. \end{aligned}$$

Note that the homogenization coefficient a_* is a scalar due to spatial symmetries of a_+. The resulting numerical value for the above discretization is

$$a_* \approx 0.1699 \,. \tag{4.6}$$

In our first example we choose the frequency ω and the incoming wave $u^{(\mathrm{in})}(x) = e^{\mathrm{i}j^{(\mathrm{in})}\cdot x}$ with

$$\omega = 0.2\pi \approx 0.628, \quad j^{(\mathrm{in})} \approx (0.440, 0.449) \,. \tag{4.7}$$

Since the frequency is quite small (and, hence, the wavelength is large), we can expect that the homogenized setting provides a good approximation.

The band structure and the level set at ω is plotted in Figure 3, where also the points j with $(j, m) \in I^{+,h}$ are marked by black dots (all very close to each other). At the selected frequency $\omega = 0.2\pi$ the band structure is only a small perturbation of a cone, which means that the band structure is similar to that of a homogenous medium. Indeed, homogenization theory provides a good qualitative prediction, as shown in Figure 4.

In our second example we choose a frequency that is relatively large:

$$\omega = 1.85, \; j^{(\mathrm{in})} \approx (1.269, 1.346). \tag{4.8}$$

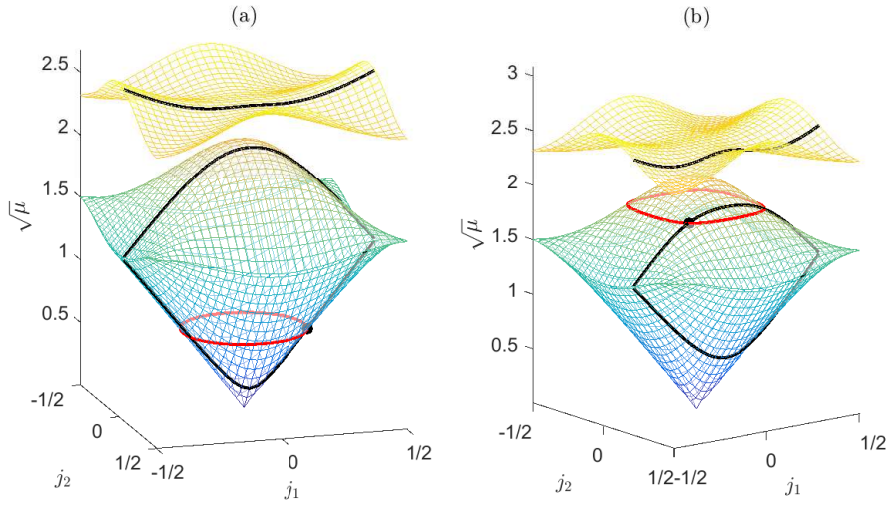

Figure 3: Band structure for a_+ given in (4.5). The three surfaces are the graphs of $\sqrt{\mu_m(j)}$ for $m = 0, 1, 2$ (identical in (a) and (b)). The red line shows points on the graph that have height ω. The black lines show points on the graph that satisfy $j_2 = j_2^{(\mathrm{in})}$. The black dots are the $(j, \sqrt{\mu})$-coordinates of the "transmission" Bloch waves $U_{\lambda_i}^{+,h}$, $i = 1, \ldots, N_{\mathrm{Bl}}$ with $\lambda_i \in I^{+,h}$ selected by the algorithm. (a) Situation for parameters ω and $j^{(\mathrm{in})}$ of (4.7). (b) Situation for the parameters of (4.8).

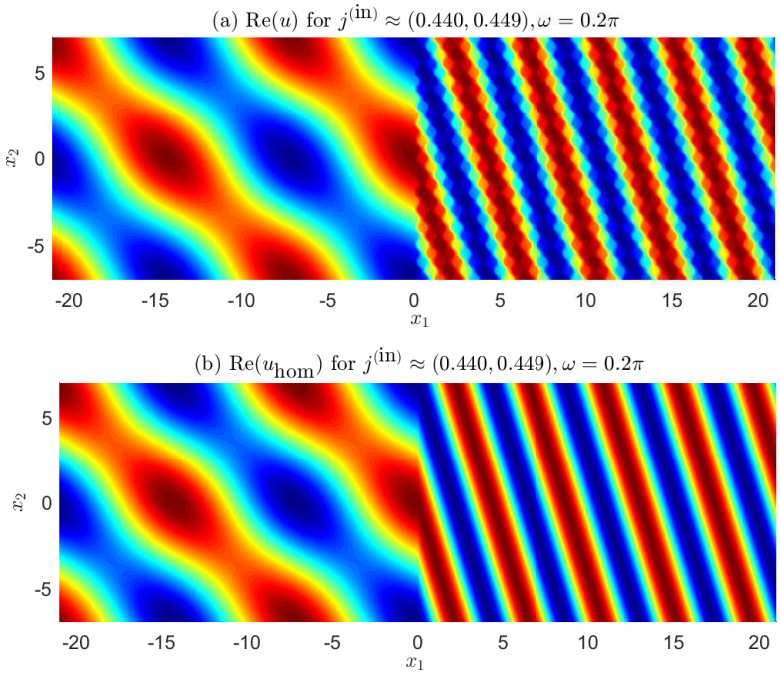

Figure 4: The color-coding shows Re(u) on Ω_{R+L}, where u is the solution to an incoming wave given by (4.7), the setting is that of Section 4.2. (a) A heterogeneous medium on the right as in (4.4); (b) A homogeneous medium on the right with the homogenized coefficient $a_* \approx 0.1699$.

The band structure at ω is far from a conical shape. Indeed, the prediction of the homogenized model is not in agreement with the solution for the heterogeneous material, see Figure 5.

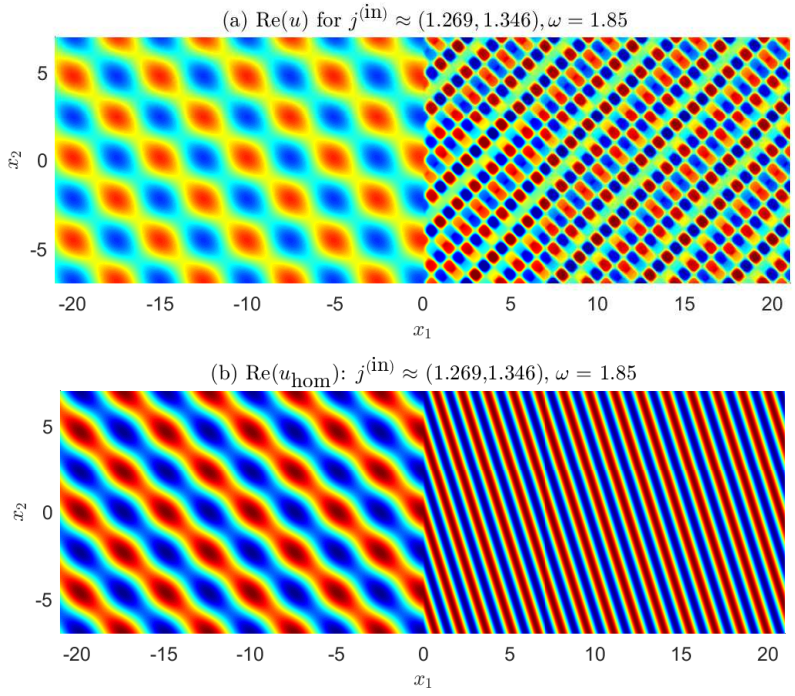

Figure 5: Re(u) for the incoming wave given by (4.8) and the setting of Section 4.2. (a) The interface from (4.4); (b) On the right half, a_+ is replaced by the homogenized coefficient $a_* \approx 0.1699$. One clearly sees negative refraction in (a), while homogenization predicts a positive refraction in (b).

The parameters in (4.8) are chosen to produce negative refraction. Negative refraction can be deduced from the negative second component of the group velocity of the "transmission" Bloch waves U_λ^+, $\lambda \in I^+$ with frequency ω. In this situation, the incoming wave propagates upwards, while the transmitted wave propagates downwards. The group velocities (multiplied by 2 for better visibility) of the "transmission" Bloch waves $U_{\lambda_i}^{+,h}$, $i = 1, \ldots, N_{\mathrm{Bl}} = 4$ with $\lambda_i \in I^{+,h}$ selected by the algorithm are plotted in Figure 6 (b). For completeness we show in Figure 6 (a) the group velocities of the "reflected Bloch waves" $U_{\lambda_i}^{-,h}$. In both (a) and (b) all four group velocity arrows lie very close to each other such that only one arrow is visible.

Refraction at interfaces between homogeneous media: Snell's law and Fresnel formulas. For a quantitative test of the numerical method we compute the analytical solution for an interface separating two homogeneous media. Here Snell's and Fresnel formulas are available and provide a reference solution. We choose the same setting as in Figure 5 (b).

For the interface with $a(x) = 1$ for $x_1 < 0$ and $a(x) = a_* > 0$ for $x_1 \geq 0$ Snell's law reads $\sqrt{a_*} = \frac{\sin\theta_+}{\sin\theta_-}$, where $\frac{1}{\sqrt{a_*}}$ is the refractive index of the material on $x_1 \geq 0$ and θ_+, θ_- are the angles between $j^{(\mathrm{out})}, j^{(\mathrm{in})}$ and the horizontal axis, respectively.

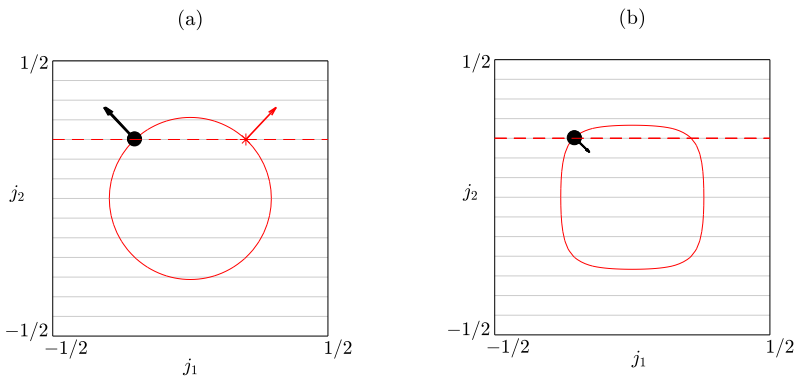

Figure 6: The Brillouin zone $\mathbb{B}$. The closed red curves mark the level set of the band structure at the level ω^2 given in (4.8) and with the setting of Section 4.2. Hence, the Bloch waves at the red points solve the Helmholtz equation with ω^2. The horizontal lines mark points that correspond to vertically periodic waves, $j_2 \in Q'_K$. The arrows show the group velocities for those waves that are relevant in the numerical result. The red arrow pointing north-east represents the incoming wave, the dashed horizontal line marks its j_2 component. This component of j_2 is preserved across the interface. (a) The situation in the left medium with the Bloch waves $U^{-,h}_{\lambda_i}$, $\lambda_i \in I^{-,h}$. (b) The situation in the right medium with the Bloch waves $U^{+,h}_{\lambda_i}, \lambda_i \in I^{+,h}$. In (b) the group velocities are multiplied by 2 for better visibility.

Here $j^{(\mathrm{out})}$ is the wavevector of the transmitted wave. For a straight vertical interface it is $j_2^{(\mathrm{out})} = j_2^{(\mathrm{in})}$, we therefore find $\frac{\sin\theta_+}{\sin\theta_-} = \frac{|j^{(\mathrm{in})}|}{|j^{(\mathrm{out})}|}$. In summary, Snell's law for this setting is

$$\sqrt{a_*} = \frac{|j^{(\mathrm{in})}|}{|j^{(\mathrm{out})}|}\,. \tag{4.9}$$

Fresnel's formulas can be derived from the continuity of u and $\partial_{x_1} u$ across the interface. Writing

$$u(x) = \begin{cases} e^{\mathrm{i}j^{(\mathrm{in})}\cdot x} + Re^{\mathrm{i}(-j_1^{(\mathrm{in})}x_1 + j_2^{(\mathrm{in})}x_2)}, & x_1 < 0, \\ Te^{\mathrm{i}j^{(\mathrm{out})}\cdot x}, & x_1 \geq 0\,, \end{cases}$$

we obtain

$$R = \frac{j_1^{(\mathrm{in})} - a_* j_1^{(\mathrm{out})}}{j_1^{(\mathrm{in})} + a_* j_1^{(\mathrm{out})}}\,, \quad \text{and} \quad T = 1 + R\,. \tag{4.10}$$

Given $j^{(\mathrm{in})}$ and a_*, (4.9) and the equation $j_2^{(\mathrm{out})} = j_2^{(\mathrm{in})}$ determine $j^{(\mathrm{out})}$, hence R and T can be evaluated from (4.10). We compare these values with the numerical ones. In the numerical results, we interpret the wavevector of the dominant Bloch wave in $I^{+,h}$ as the vector $j^{(\mathrm{out})}$. We denote the correspoding index in $I^{+,h}$ by λ_{out}. Similarly, we denote by λ_{refl} the index of the dominant Bloch wave in $I^{-,h}$. The coefficients R and T are approximated by the coefficient of the basis functions $U^{-,h}_{\lambda_{\mathrm{refl}}}$ and $U^{+,h}_{\lambda_{\mathrm{out}}}$, respectively (after renormalizing $U^{-,h}_{\lambda_{\mathrm{refl}}}$ and $U^{+,h}_{\lambda_{\mathrm{out}}}$ such that $\|U^{-,h}_{\lambda_{\mathrm{refl}}}\|_{L^2([0,1]^2)} = \|U^{+,h}_{\lambda_{\mathrm{out}}}\|_{L^2([0,1]^2)} = 1$). We denote these coefficients α_{refl} and α_{out}, respectively.

We use the incoming field as in Figure 5 (b), i.e. that given in (4.8). Discretizing with $h_1 = 0.05$ and $h_2 \approx 0.0526$, we get $a_* \approx 0.1699$ ($\sqrt{a_*} \approx 0.4122$) and $\frac{|j^{(\mathrm{in})}|}{|j^{(\mathrm{out})}|} \approx$

0.414383. This approximation improves when the FEM-discretization is refined. In Figure 7 we plot the errors $|R - |\alpha_{\text{refl}}||$ and $|T - |\alpha_{\text{out}}||$ for the absorption parameter values $\delta = 10^{-p}, p = 2, 3, 4, 5, 6$. For δ even smaller the errors do not decrease due to the dominance of the discretization error. By refining the discretization, the error for $\delta < 10^{-6}$ can be made smaller.

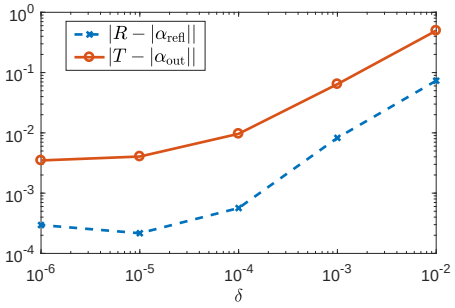

Figure 7: Convergence of the error in the reflection and transmission coefficients R and T with respect to δ.

4.3 Numerical results II: Scattering and negative refraction with a localized source

In these tests we consider the same interface as in Section 4.2. Instead of an incoming field we investigate a spatially localized source; we choose

$$f(x) = 2e^{-3|x-x_*|^2}, \ x_* = (-3.5, 0). \tag{4.11}$$

This source generates waves in all directions, hence a relatively large number N_{Bl} of Bloch basis functions is needed. We consider a vertically wide domain in order for the periodic boundary conditions to have a smaller effect near the source location. The domain is given by $H = 100$, $\varepsilon = 1$, $\varepsilon R = 45$, $\varepsilon L = 15$, and we set $N_{\text{Bl}} = 180$. We choose again $\omega = 1.85$. Figure 8 shows the solution modulus for $h_1 = h_2 = 0.0625$. In the crystal, close to the interface, the field is clearly focused in a strip near the central line. We interpret that this effect is generated by the negative refraction at the selected frequency.

In Figure 9 we plot once more the group velocities of the Bloch waves $U^{-,h}_{\lambda_i}$, $\lambda_i \in I^{-,h}$ in (a) and of $U^{+,h}_{\lambda_i}$, $\lambda_i \in I^{+,h}$ in (b). The size of the dots at the foot of each arrow is proportional to the relative modulus of the coefficient of the Bloch wave $U^{-,h}_{\lambda_i}$ in (a) and $U^{+,h}_{\lambda_i}$ in (b). The strength of each Bloch wave in the solution u is thus visualized. Note that the large vertical size H leads to a large set Q'_K, which explains the large number of gray horizontal lines in Figure 9.

In order to confirm the lensing effect of a crystal for frequencies with negative refraction, we use the same source as above but truncate the crystal after 10 horizontal periods, see Figure 10. With the frequency $\omega = 0.2\pi \approx 0.628$, where the refraction is positive, no focusing occurs; contrastingly, at $\omega = 1.85$, a focused image is seen on the right side of the crystal. This confirms findings of [25]. We use here $\varepsilon = 1$, $\varepsilon R = 27$, $\varepsilon L = 9$, $H = 60$, $h_1 \approx 0.0769$, $h_2 \approx 0.0714$, and $N_{\text{Bl}} = 80$.

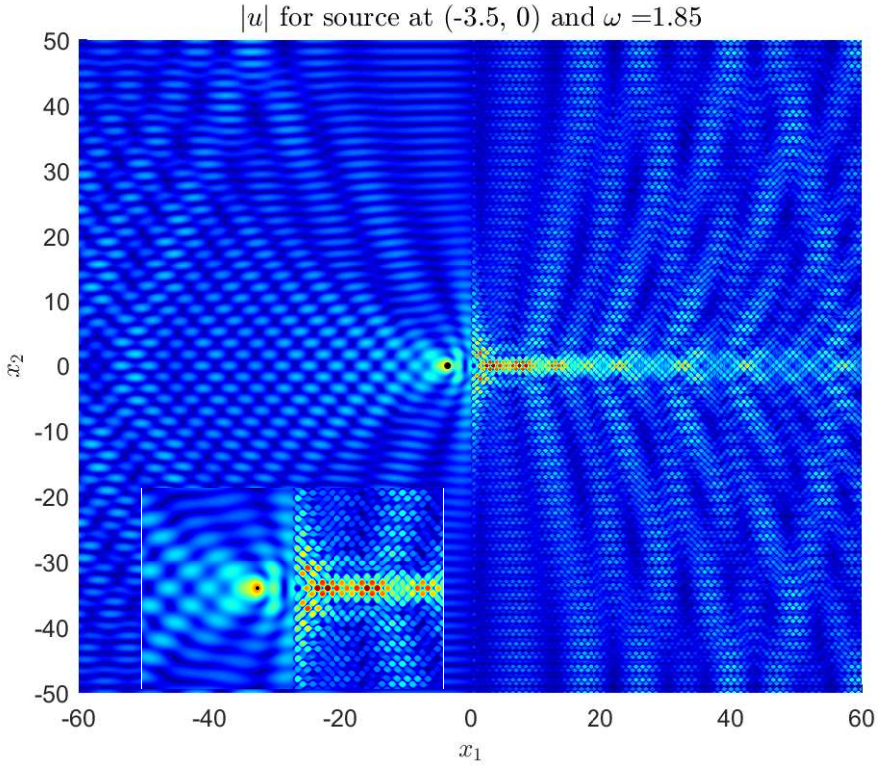

Figure 8: $|u|$ for the scattering problem with the Gaussian source (4.11). The interface is as in (4.4), $\omega = 1.85$ and $N_{\mathrm{Bl}} = 180$, $\varepsilon R = 45$, $\varepsilon L = 15$, $\varepsilon = 1$, $H = 100$, $h_1 = h_2 = 0.0625$. The inset zooms in on the vicinity of the center (near the source location).

Acknowledgements

Support of the first author by the DFG grant DO1467/3-1 and of the second author by the DFG grant Schw 639/6-1 is gratefully acknowledged.

References

[1] G. Allaire and C. Conca. Bloch wave homogenization and spectral asymptotic analysis. *J. Math. Pures Appl. (9)*, 77(2):153–208, 1998.

[2] H. W. Alt. *Linear functional analysis*. Universitext. Springer-Verlag London, Ltd., London, 2016. An application-oriented introduction, Translated from the German edition by Robert Nürnberg.

[3] A.-S. Bonnet-Ben Dhia, G. Dakhia, C. Hazard, and L. Chorfi. Diffraction by a defect in an open waveguide: a mathematical analysis based on a modal radiation condition. *SIAM J. Appl. Math.*, 70(3):677–693, 2009.

[4] G. Bouchitté and D. Felbacq. Negative refraction in periodic and random photonic crystals. *New J. Phys*, 7(159, 10.1088), 2005.

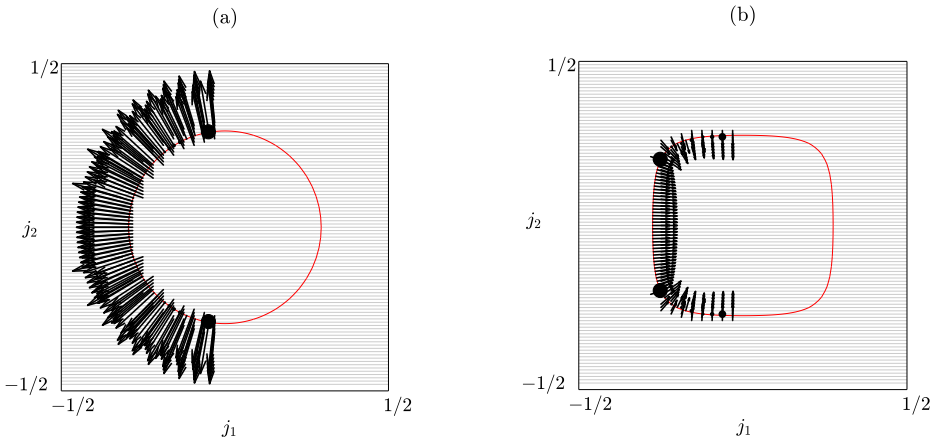

Figure 9: The Brillouin zone for the scattering problem of Figure 8, the symbols are as in Figure 6, (a) showing the left medium and (b) the right medium. In contrast to the case of a single incoming wave, the numerical solution now uses many different Bloch waves, indicated by the arrows. Since all waves in $I^{\pm,h}$ are outgoing, all arrows point to the left in the left medium and to the right in the right medium. The size of the dots at the foot of each arrow is porportional to the modulus of the coefficient of each Bloch wave.

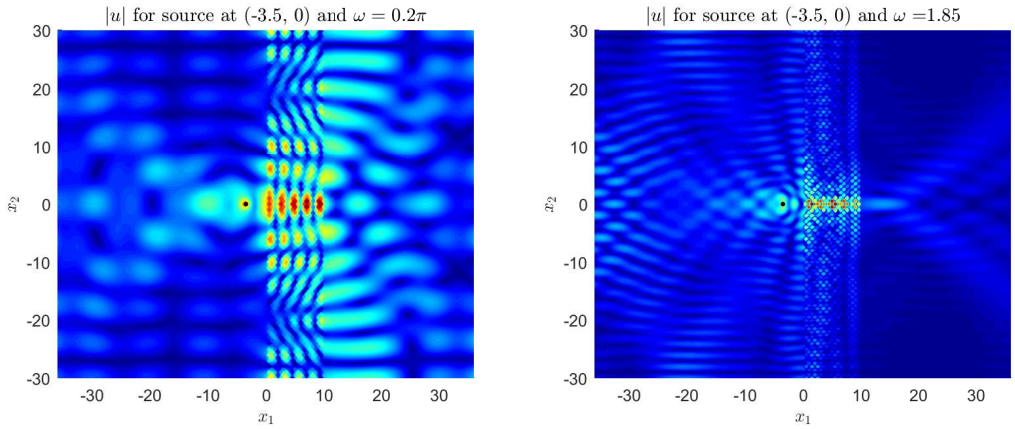

Figure 10: $|u|$ for the scattering problem with the Gaussian source (4.11) and a crystal of thickness 10ε, $\varepsilon = 1$. The material in $x_1 \in [0, 10\varepsilon]$ is given by a_+ in (4.5) and by 1 in $x_1 \notin [0, 10\varepsilon]$. We use $N_{\mathrm{Bl}} = 80$, $H = 60$, $\varepsilon R = 27$, $\varepsilon L = 9$, and $h_1 \approx 0.0769$, $h_2 \approx 0.0714$. Left: Frequency $\omega = 0.2\pi \approx 0.628$ leading to a positive refraction. Right: Frequency $\omega = 1.85$ with a negative refraction and a resulting lensing effect.

[5] G. Bouchitté and B. Schweizer. Homogenization of Maxwell's equations in a split ring geometry. *Multiscale Model. Simul.*, 8(3):717–750, 2010.

[6] C. Conca and M. Vanninathan. Homogenization of periodic structures via Bloch decomposition. *SIAM J. Appl. Math.*, 57(6):1639–1659, 1997.

[7] T. Dohnal, A. Lamacz, and B. Schweizer. Bloch-wave homogenization on large time scales and dispersive effective wave equations. *Multiscale Modeling & Simulation*, 12(2):488–513, 2014.

[8] A. Efros and A. Pokrovsky. Dielectric photonic crystal as medium with negative electric permittivity and magnetic permeability. *Solid State Communications*, 129:643–647, 2004.

[9] S. Fliss. A Dirichlet-to-Neumann approach for the exact computation of guided modes in photonic crystal waveguides. *SIAM J. Sci. Comput.*, 35(2):B438–B461, 2013.

[10] S. Fliss and P. Joly. Exact boundary conditions for time-harmonic wave propagation in locally perturbed periodic media. *Applied Numerical Mathematics*, 59(9):2155 – 2178, 2009.

[11] S. Fliss and P. Joly. Wave propagation in locally perturbed periodic media (case with absorption): numerical aspects. *J. Comput. Phys.*, 231(4):1244–1271, 2012.

[12] S. Fliss and P. Joly. Solutions of the time-harmonic wave equation in periodic waveguides: asymptotic behaviour and radiation condition. *Arch. Ration. Mech. Anal.*, 219(1):349–386, 2016.

[13] S. Fliss, D. Klindworth, and K. Schmidt. Robin-to-Robin transparent boundary conditions for the computation of guided modes in photonic crystal wave-guides. *BIT*, 55(1):81–115, 2015.

[14] H. Helmholtz. Theorie der Luftschwingungen in Röhren mit offenen Enden. *J. Reine Angew. Math.*, 57:1–72, 1860.

[15] V. Hoang. The limiting absorption principle for a periodic semi-infinite waveguide. *SIAM J. Appl. Math.*, 71(3):791–810, 2011.

[16] V. Hoang and M. Radosz. Absence of bound states for waveguides in two-dimensional periodic structures. *J. Math. Phys.*, 55(3):033506, 20, 2014.

[17] T. Hohage, F. Schmidt, and L. Zschiedrich. Solving time-harmonic scattering problems based on the pole condition. I. Theory. *SIAM J. Math. Anal.*, 35(1):183–210, 2003.

[18] J. Joannopoulos, S. Johnson, J. Winn, and R. Meade. *Photonic Crystals – Molding the Flow of Light*. Princeton University Press, 2008.

[19] P. Joly, J.-R. Li, and S. Fliss. Exact boundary conditions for periodic waveguides containing a local perturbation. *Commun. Comput. Phys.*, 1, 2006.

[20] S. Kaulmann, M. Ohlberger, and B. Haasdonk. A new local reduced basis discontinuous galerkin approach for heterogeneous multiscale problems. *Comptes Rendus Mathematique*, 349(23):1233 – 1238, 2011.

[21] P. Kuchment. The mathematics of photonic crystals. In *Mathematical modeling in optical science*, volume 22 of *Frontiers Appl. Math.*, pages 207–272. SIAM, Philadelphia, PA, 2001.

[22] A. Lamacz and B. Schweizer. Effective Maxwell equations in a geometry with flat rings of arbitrary shape. *SIAM J. Math. Anal.*, 45(3):1460–1494, 2013.

[23] A. Lamacz and B. Schweizer. A negative index meta-material for Maxwell's equations. *SIAM J. Math. Anal.*, 48(6):4155–4174, 2016.

[24] A. Lamacz and B. Schweizer. Outgoing wave conditions in photonic crystals and transmission properties at interfaces. *TU Dortmund*, submitted, 2016.

[25] C. Luo, S. G. Johnson, J. D. Joannopoulos, and J. B. Pendry. All-angle negative refraction without negative effective index. *Phys. Rev. B*, 65:201104, May 2002.

[26] S. A. Nazarov. Umov-Mandel′shtam radiation conditions in elastic periodic waveguides. *Mat. Sb.*, 205(7):43–72, 2014.

[27] G. Papanicolau, A. Bensoussan, and J. Lions. *Asymptotic Analysis for Periodic Structures*. Studies in Mathematics and its Applications. Elsevier Science, 1978.

[28] J. Pendry. Negative refraction makes a perfect lens. *Phys. Rev. Lett.*, 85(3966), 2000.

[29] A. Pokrovsky and A. Efros. Diffraction theory and focusing of light by a slab of left-handed material. *Physica B: Condensed Matter*, 338(1–4):333–337, 2003.

[30] M. Radosz. New limiting absorption and limit amplitude principles for periodic operators. *Z. Angew. Math. Phys.*, 66(2):253–275, 2015.

[31] T. Strouboulis, I. Babuška, and R. Hidajat. The generalized finite element method for helmholtz equation: Theory, computation, and open problems. *Computer Methods in Applied Mechanics and Engineering*, 195(37):4711 – 4731, 2006. John H. Argyris Memorial Issue. Part I.

Preprints ab 2013/12

2017-03 **Tomáš Dohnal and Ben Schweizer**
A Bloch wave numerical scheme for scattering problems in periodic wave-guides

2017-02 **Matthias Röger and Ben Schweizer**
Strain gradient visco-plasticity with dislocation densities contributing to the energy

2017-01 **Ben Schweizer and Maik Urban**
Effective Maxwell´s equations in general periodic microstructures

2016-05 **Robert Lipton and Ben Schweizer**
Effective Maxwell´s equations for perfectly conducting split ring resonators

2016-04 **Ben Schweizer**
Resonance meets homogenization - Construction of meta-materials with astonishing properties

2016-03 **Ben Schweizer**
On Friedrichs inequality, Helmholtz decomposition, vector potentials, and the div-curl lemma

2016-02 **Michael Voit**
Generalized commutative association schemes, hypergroups, and positive product formulas

2016-01 **Agnes Lamacz and Ben Schweizer**
Effective acoustic properties of a meta-material consisting of small Helmholtz resonators

2015-13 **Christian Eggert, Ralf Gäer, Frank Klinker**
The general treatment of non-symmetric, non-balanced star circuits: On the geometrization of problems in electrical metrology

2015-12 **Daniel Kobe and Jeannette H.C. Woerner**
Oscillating Ornstein-Uhlenbeck processes and modelling electricity prices

2015-11 **Sven Glaser**
A distributional limit theorem for the realized power variation of linear fractional stable motions

2015-10 **Herold Dehling, Brice Franke and Jeannette H.C. Woerner**
Estimating drift parameters in a fractional Ornstein Uhlenbeck process with periodic mean

2015-09 **Harald Garcke, Johannes Kampmann, Andreas Rätz and Matthias Röger**
A coupled surface-Cahn-Hilliard bulk-diffusion system modeling lipid raft formation in cell membrans

2015-08 **Agnes Lamacz and Ben Schweizer**
Outgoing wave conditions in photonic crystals and transmission properties at interfaces

2015-07 **Manh Hong Duong, Agnes Lamacz, Mark A. Peletier and Upanshu Sharma**
Variational approach to coarse-graining of generalized gradient flows

2015-06 **Agnes Lamacz and Ben Schweizer**
A negative index meta-material for Maxwell´s equations

2015-05 **Michael Voit**
Dispersion and limit theorems for random walks associated with hypergeometric functions of type *BC*

2015-04 **Andreas Rätz**
Diffuse-interface approximations of osmosis free boundary problems

2015-03 **Margit Rösler and Michael Voit**
A multivariate version of the disk convolution

2015-02 **Christina Dörlemann, Martin Heida, Ben Schweizer**
Transmission conditions for the Helmholtz-equation in perforated domains

2015-01 **Frank Klinker**
Program of the International Conference
Geometric and Algebraic Methods in Mathematical Physics
March 16-19, 2015, Dortmund

2014-10 **Frank Klinker**
An explicit description of SL (2, $\mathbb{C}$) in terms of $SO^{+}(3, 1)$ and vice versa

2014-09 **Margit Rösler and Michael Voit**
Integral representation and sharp asymptotic results for some Heckman-Opdam hypergeometric functions of type BC

2014-08 **Martin Heida and Ben Schweizer**
Stochastic homogenization of plasticity equations

2014-07 **Margit Rösler and Michael Voit**
A central limit theorem for random walks on the dual of a compact Grassmannian

2014-06 **Frank Klinker**
Eleven-dimensional symmetric supergravity backgrounds, their geometric superalgebras, and a common reduction

2014-05 **Tomáš Dohnal and Hannes Uecker**
Bifurcation of nonlinear Bloch waves from the spectrum in the Gross-Pitaevskii equation

2014-04 **Frank Klinker**
A family of non-restricted $D = 11$ geometric supersymmetries

2014-03 **Martin Heida and Ben Schweizer**
Non-periodic homogenization of infinitesimal strain plasticity equations

2014-02 **Ben Schweizer**
The low frequency spectrum of small Helmholtz resonators

2014-01 **Tomáš Dohnal, Agnes Lamacz, Ben Schweizer**
Dispersive homogenized models and coefficient formulas for waves in general periodic media

2013-16 **Karl Friedrich Siburg**
Almost opposite regression dependence in bivariate distributions

2013-15 **Christian Palmes and Jeannette H. C. Woerner**
The Gumbel test and jumps in the volatility process

2013-14 **Karl Friedrich Siburg, Katharina Stehling, Pavel A. Stoimenov, Jeannette H. C. Wörner**
An order for asymmetry in copulas, and implications for risk management

2013-13 **Michael Voit**
Product formulas for a two-parameter family of Heckman-Opdam hypergeometric functions of type BC

2013-12 **Ben Schweizer and Marco Veneroni**
Homogenization of plasticity equations with two-scale convergence methods